Published in final edited form as:

Science. 2017 September 08; 357(6355): 1033–1036. doi:10.1126/science.aan3846.

Behavioral time scale synaptic plasticity underlies CA1 place fields

Katie C. Bittner[1,*], **Aaron D. Milstein**[1,2,*], **Christine Grienberger**[1], **Sandro Romani**[1], **Jeffrey C. Magee**[1,†]

[1]Howard Hughes Medical Institute, Janelia Research Campus, Ashburn, VA 20147, USA.

[2]Department of Neurosurgery, Stanford University School of Medicine, Stanford, CA 94305, USA.

Abstract

Learning is primarily mediated by activity-dependent modifications of synaptic strength within neuronal circuits. We discovered that place fields in hippocampal area CA1 are produced by a synaptic potentiation notably different from Hebbian plasticity. Place fields could be produced in vivo in a single trial by potentiation of input that arrived seconds before and after complex spiking. The potentiated synaptic input was not initially coincident with action potentials or depolarization. This rule, named behavioral time scale synaptic plasticity, abruptly modifies inputs that were neither causal nor close in time to postsynaptic activation. In slices, five pairings of subthreshold presynaptic activity and calcium (Ca^{2+}) plateau potentials produced a large potentiation with an asymmetric seconds-long time course. This plasticity efficiently stores entire behavioral sequences within synaptic weights to produce predictive place cell activity.

The most influential theory concerning the physiological basis of learning and memory posits the following: If activity in a presynaptic neuron “repeatedly or persistently takes part in firing” a postsynaptic neuron, the strength of their connections should be increased (1). The two core elements of Hebb’s postulate, causality and repetition, have shaped synaptic plasticity experiments and learning theories for decades (2-5). Hebb’s rule, as implemented through dozens of essentially coincident activations of pre- and postsynaptic neurons, has been proposed to underlie autonomous or unsupervised learning in a wide range of brain regions and across multiple species (3-12). However, these two core elements also produce some of the most persistent challenges in biological learning, that is, how can associations be formed over behavioral time scales (seconds versus milliseconds) and in just a few experiences (single versus dozens of trials) to generate useful predictions of the future (2, 3, 7, 11, 13-15).

Despite decades of research, there is little direct evidence concerning the actual learning rules in place within different brain regions. For example, the hippocampus plays a role in many forms of memory (16-18) and synaptic plasticity was first observed and has been most

†Corresponding author. mageej@janelia.hhmi.org.
*These authors contributed equally to this work.

SUPPLEMENTARY MATERIALS
www.sciencemag.org/content/357/6355/1033/suppl/DC1

intensively studied there (6-8, 10). Yet, the plasticity rules shaping hippocampal activity remain unknown, and computational studies suggest standard rules need modification (7, 10, 18).

We therefore determined the plasticity rules that shape place-field formation in hippocampal area CA1. New CA1 place fields can be rapidly formed anywhere in a spatial environment when the initiation of complex spiking by dendritic Ca^{2+} plateau potentials drives an increase in the weights of excitatory synaptic inputs (19, 20). We used intracellular recordings from CA1 pyramidal neurons of head-fixed mice running laps on a linear-track treadmill (see supplementary methods). All recorded neurons initially were silent cells in that they did not show any location-specific firing for at least the first 5 min of the recording. After this baseline period, plateau potential initiation [either naturally occurring (n = 7) or experimentally induced (n = 20)] produced a ramp-like depolarization of membrane potential (V_m ramp) that was observed to drive place-field firing on subsequent trials (19-22) (Fig. 1A to C, and fig. S1). The average number of trials containing plateau potentials during the induction phase was 1.4 ± 0.22 for naturally occurring and 5.1 ± 0.32 for experimentally induced place fields. The induced V_m ramps extended back in time (mean time to start of V_m ramp, 3.8 ± 0.2 s; n = 27; Fig. 1B and fig. S2) to locations along the track where the postsynaptic cell did not exhibit any action potential (AP) firing during the plasticity induction trials (average spatial firing rate for 180 cm preceding plateau; 0.1 ± 0.05 Hz, n = 27; Fig. 1A to C, and fig. S2), or even somatic depolarization compared to nonpotentiated regions (mean V_m for initial 20 cm of V_m ramp, −60.3 ± 0.04 mV versus preceding 20 cm, −59.6 ± 0.4 mV; P = 0.34; Fig. 1B and C, and fig. S2).

This suggests that the learning rule responsible for input potentiation could span a much longer time (seconds) than predicted by standard rules (tens of milliseconds) to include inputs that were not directly involved in driving neuronal firing. Because CA3 provides position-specific place cell input to CA1 (23), a plasticity rule that operates on seconds-long time scales predicts that the faster mice run during the induction trial, the wider the resulting V_m ramps (Fig. 1D to F). For a standard rule spanning only tens of milliseconds, the distances covered would not vary substantially (Fig. 1E and F, and red line in G). We looked at the relationship between the width of the V_m ramp and the running speed of the mouse during the induction trial(s), and indeed, the faster the mouse ran during the induction trial(s), the greater the V_m ramp width (Fig. 1G). The slope of this relationship was on the order of seconds [Fig. 1G, gray line, goodness of fit (r^2) = 0.76, m = 2.5 s], confirming the existence of a plasticity rule operating on a seconds-long time scale (see supplementary methods). Once the CA1 V_m ramp was established, ramp width was not related to an animal's running speed during the trials that followed the induction, as expected for place cell firing (24) (average width of slow trials versus fast trails; 125.4 ± 7.1 versus 126.5 ± 6.6 cm, n = 22; P = 0.62; Fig. 1H).

We next sought to quantitatively study the shape of this synaptic plasticity rule and how it relates in time to the plateau potential. We deconvolved the V_m ramps from our intracellular CA1 recordings with a synaptic input pattern based on the movement of the animal during trials containing plateau potentials (Fig. 2A and B; see supplementary methods). We observed an asymmetric plasticity kernel that was two-orders-of-magnitude longer than that

expected for standard plasticity (kernel rise time extending for ~3 s, decay time ~2 s) (Fig. 2C to E). The analysis successfully captured the experimentally observed variation in V_m ramp width (fig. S3). These results indicate that CA1 place cells are produced by a learning rule that asymmetrically projects for seconds in both directions around the postsynaptic activation that induced the plasticity (fig. S4). This time course allows inputs that were neither directly causal nor even temporally contiguous with postsynaptic activation (either APs or plateau potentials) to become potentiated, and the magnitude of this potentiation permits this to occur without substantial repetition. The time course also produces V_m depolarizations that have a predictive quality, in that they peak and have a center of mass well before the actual induction location (fig. S1, see supplementary methods). The rule that shapes activity in area CA1 thus does not conform to Hebb's postulate.

To determine if the above plasticity rule could be observed under more realistic model conditions, we constructed and optimized a biophysically detailed model and attempted to fully account for the experimental data. In this model, a local signal that rises and decays with a slow time course (τ_{rise} = 212.9 ± 38.8 ms, τ_{decay} = 1196.4 ± 170.9 ms) is generated at each activated synapse even though the input remains subthreshold for output. This signal on its own does not result in synaptic potentiation (2). However, a second more global signal (τ_{rise} = 101.5 ± 21.1 ms, τ_{decay} = 454.8 ± 76.8 ms) is produced by dendritic plateau potentials, and the overlap between the local and global signals determines the degree of synaptic weight change at each input (Fig. 2F and fig. S5). The plasticity produced in this model was asymmetric with respect to the plateau potential and covered a similarly long duration time span (rise time = ~4 s, decay time = ~3 s; Fig. 2G), as found in the above nonparametric analysis. The model could recapitulate the variation in all observed features of the induced V_m ramps (Fig. 2H and fig. S5), whereas an alternative version that used short duration local and global signals (τ_{rise} = 10 ms, t_{decay} = 100 ms) was not successful (Fig. 2H). Further, the model makes obvious why long-duration plateaus are far more effective than brief APs at generating a global signal capable of interacting with the proposed local signal. We termed this new plasticity behavioral time scale synaptic plasticity (BTSP).

Because no such synaptic plasticity has been reported for CA1 pyramidal neurons, or any cortical cell type, we explored whether this phenomenon could be reproduced in hippocampal slice preparations from adult mice. We devised whole-cell patch-clamp conditions using Cs^{2+} internal solutions to enable the initiation of plateau potentials independent of synaptic input (25) (see supplementary methods). Area CA3 was removed from the slices to silence spontaneous activity, and electrical stimulation of stratum radiatum axons was used to simulate "spatially tuned" subthreshold synaptic inputs onto CA1 pyramidal cells (10 synaptic stimuli delivered at 10 Hz). This was paired with a postsynaptic plateau potential that was generated through somatic current injection alone (300 ms, 300- to 600-pA current injection) and delivered either synchronously or separated in time with intervals ranging from At = Δt = −3250 ms (presynaptic before postsynaptic) to Δt = +2250 ms (presynaptic after postsynaptic) in different neurons (n = 58; Fig. 3A to F, and figs. S6 and S7). We used only five pairings (15-s interval; average lap time = 15.4 ± 1.7 s, n = 20) to mirror the plasticity seen in behaving animals, which could be produced in as few as one induction. Changes in synapse strength were quantified with paired-pulse excitatory

postsynaptic potentials (EPSPs) (50 ms interval; 0.05 Hz) that were monitored for a baseline period of 10 to 15 min (first EPSP amplitude = 2.4 ± 0.11 mV, $n = 63$) and for up to 60 min following induction (fig. S6C). We observed a large, approximately threefold potentiation (3.12 ± 0.11, $n = 4$) upon coincident stimulation ($\Delta t = 0$ ms) that decayed gradually with Δt, remaining significant for nearly 4 s in the backward Δt direction (presynaptic before postsynaptic: $\tau_b = 1.31 \pm 0.22$ s SD, $n = 42$) and more than 2 s in the forward Δt direction (postsynaptic before presynaptic: $\tau_f = 0.69 \pm 0.11$ s SD, $n = 20$) (Fig. 3G and figs. S6 and S7). Potentiation stabilized minutes after induction and persisted for the duration of the recordings (Fig. 3C and D, and figs. S6 and S7). No changes in input resistance were observed (baseline: 83.8 ± 2.9 MΩ; postpairing: 82.2 ± 2.6 MΩ; $n = 58$, $P = 0.69$ paired two-tailed t test for intervals ±1500 ms; Fig. 3H). A relatively small decrease in paired-pulse facilitation, though statistically significant (baseline: 2.14 ± 0.08; postpairing: 1.99 ± 0.07; $n = 58$, $P = 0.01$ paired two-tailed t test for intervals ±1500 ms; Fig. 3H), suggests a predominantly postsynaptic mechanism of action. BTSP was pathway specific, as a second nonstimulated control pathway did not significantly potentiate following application of the pairing protocol to a test pathway (500 ms interval; control path: 1.08 ± 0.19 postpairing/baseline, $n = 6$, $P = 0.21$; test path: 1.87 ± 0.26 postpairing/baseline, $n = 6$, $P = 0.0005$; fig. S8).

We next tested the pharmacological sensitivity of BTSP to identify the main molecular components involved. BTSP was sensitive to *N*-methyl-D-aspartate receptor (NMDAR) blockade because 20 μM D-aminophosphovalerate (D-APV) reduced the amplitude of the potentiation at the −750-ms pairing interval by 84% (control: 2.16 ± 0.15; drug: 1.19 ± 0.03; $n = 6$, $P = 0.00033$) (Fig. 4A and B). The potentiation remaining after D-APV treatment, particularly just after pairing, may be responsible for the degraded, unstable place fields reported in novel spatial environments during NMDAR antagonism (26). The L-type Ca^{2+} channel blocker, nimodipine (10 μM), also inhibited the potentiation at this same pairing interval (73% inhibition; control: 2.16 ± 0.15; drug: 1.31 ± 0.04; $n = 6$, $P = 0.0011$) (Fig. 4A and B). The blockade of potentiation by D-APV and nimodipine was not mediated by a reduced duration of the induction plateau potentials (plateau duration: control, 204.7 ± 18.0 ms, $n = 15$; nimodipine: 236.7 ± 29.6 ms, $n = 6$,$P = 0.33$; D-APV: 200.5 ms, $n = 6$, $P = 0.91$) (Fig. 4C). A similar pharmacological profile has been reported for another form of long-term potentiation induced by dendritic spikes in CA1 pyramidal neurons (27). Finally, we examined the effect of nimodipine on place-field induction during in vivo recordings. Pressure application of nimodipine around the neuron under study (see supplementary methods) significantly reduced the amplitude of the V_m ramp induced by plateau-potential initiation compared to vehicle controls (V_m ramp amplitude: vehicle, 6.2 ± 1.3 mV, $n = 6$; 5 μM nimodipine, 1.3 ± 0.4 mV, $n = 5$; $P = 0.042$) (Fig. 4D and E). Plateau-potential duration was likewise unchanged by nimodipine under these conditions (control: 264.7 ± 15.3 ms, $n = 6$; nimodipine: 250.6 ± 16.7 ms, $n = 5$, $P = 0.41$) (Fig. 4F). These experimental results directly link BTSP with place-field formation in area CA1. They also illuminate the potential mechanisms generating the long-duration signals present in the above realistic model (28-30). However, extensive future studies are needed to determine the specific signaling pathways involved.

A noteworthy type of synaptic plasticity underlies neuronal activity in hippocampal area CA1. Although BTSP exhibits associativity and specificity, it nevertheless leads to the potentiation of inputs that are neither causal nor even close in time with complex spiking. Moreover, the magnitude of the induced plasticity is such that it can abruptly form new place fields in just a single trial. We speculate that complex spiking may be enhanced by unfamiliar events, rewards, or punishments. Hence, the BTSP induction mechanism may operate as an instructive-type signal, promoting learning that is neither autonomous nor correlative.

BTSP can rapidly store the entire sequence of events that occurred for several seconds before and after plateau-potential initiation within the synaptic weights of area CA1. The potent, asymmetric seconds-long plasticity produces, within a single run, place-field firing that peaks before the location where complex spiking occurred, providing a predictive signal of behaviorally relevant events (fig. S9). Such experience-dependent tailoring of the CA1 representation by BTSP could create network-level overrepresentations of particularly important locations as well as the activation of specific trajectories toward reward locations observed during different phases of exploration (31-34). In addition, various forms of hippocampal-dependent learning such as that observed during episodic memory and trace conditioning would greatly benefit from a storage mechanism operating on seconds-long time scales (35, 36). More generally, BTSP represents a plausible biophysical implementation of plasticity rules proposed in numerous theoretical studies in systems neuroscience and machine learning (2, 3, 7, 11, 13-15). In particular, the linking of past synaptic input and neuronal activation by dendritic plateaus alleviates the need for prolonged internal stimulus representations (13-15). Thus, BTSP may provide a more straightforward physiological basis for many types of learning than plasticity that explicitly conforms to Hebb’s postulate.

Supplementary Material

Refer to Web version on PubMed Central for supplementary material.

ACKNOWLEDGMENTS

We thank M. Tadross, G. Tervo, and I. Soltesz for discussions and N. Brunel, J. Dudman, R. Gutig, G. Rubin, and M. Tadross for comments on the manuscript. This work is supported by HHMI and NIH BRAIN (Brain Research through Advancing Innovative Neurotechnologies) grant NS090583. Data are archived on Janelia Research Campus servers and are available upon request.

REFERENCES AND NOTES

1. Hebb DO, The Organization of Behavior (Wiley, 1949).
2. Sutton RS, Barto AG, Psychol. Rev. 88, 135–170 (1981). [PubMed: 7291377]
3. Dayan P, Abbott L, Theoretical Neuroscience (MIT Press, 2001).
4. Mayford M, Siegelbaum SA, Kandel ER, Cold Spring Harb. Perspect. Biol. 4, a005751 (2012). [PubMed: 22496389]
5. Feldman DE, Neuron 75, 556–571 (2012). [PubMed: 22920249]
6. Bliss TV, Lomo T, J. Physiol 232, 331–356 (1973). [PubMed: 4727084]
7. Blum KI, Abbott LF, Neural Comput. 8, 85–93 (1996). [PubMed: 8564805]
8. Magee JC, Johnston D, Science 275, 209–213 (1997). [PubMed: 8985013]

9. Markram H, Lübke J, Frotscher M, Sakmann B, Science 275, 213–215 (1997). [PubMed: 8985014]
10. Foster DJ, Morris RGM, Dayan P, Hippocampus 10, 1–16 (2000). [PubMed: 10706212]
11. Izhikevich EM, Cereb. Cortex 17, 2443–2452 (2007). [PubMed: 17220510]
12. Cassenaer S, Laurent G, Nature 482, 47–52 (2012). [PubMed: 22278062]
13. Hull CL, Principles of Behavior (Appleton-Century, New York, 1943).
14. Montague PR, Dayan P, Sejnowski TJ, J. Neurosci 16, 1936–1947 (1996). [PubMed: 8774460]
15. Drew PJ, Abbott LF, Proc. Natl. Acad. Sci. U.S.A 103, 8876–8881 (2006). [PubMed: 16731625]
16. Scoville WB, Milner B, J. Neurol. Neurosurg. Psychiatry 20, 11–21 (1957). [PubMed: 13406589]
17. Squire LR, Neurobiol. Learn. Mem 82, 171–177 (2004). [PubMed: 15464402]
18. Foster D, Knierim J, Curr. Opin. Neurobiol 22, 294–300 (2012). [PubMed: 22226994]
19. Bittner KC et al., Nat. Neurosci 18, 1133–1142 (2015). [PubMed: 26167906]
20. Grienberger C, Milstein AD, Bittner KC, Romani S, Magee JC, Nat. Neurosci 20, 417–426 (2017). [PubMed: 28114296]
21. Harvey CD, Collman F, Dombeck DA, Tank DW, Nature 461, 941–946 (2009). [PubMed: 19829374]
22. Lee D, Lin B-J, Lee AK, Science 337, 849–853 (2012). [PubMed: 22904011]
23. Mizuseki K, Royer S, Diba K, Buzsáki G, Hippocampus 22, 1659–1680 (2012). [PubMed: 22367959]
24. Geisler C, Robbe D, Zugaro M, Sirota A, Buzsáki G, Proc. Natl. Acad. Sci. U.S.A 104, 8149–8154 (2007). [PubMed: 17470808]
25. Takahashi H, Magee JC, Neuron 62, 102–111 (2009). [PubMed: 19376070]
26. Kentros C et al., Science 280, 2121–2126 (1998). [PubMed: 9641919]
27. Remy S, Spruston N, Proc. Natl. Acad. Sci. U.S.A 104, 17192–17197 (2007). [PubMed: 17940015]
28. Harvey CD, Yasuda R, Zhong H, Svoboda K, Science 321, 136–140 (2008). [PubMed: 18556515]
29. Lee SJ, Escobedo-Lozoya Y, Szatmari EM, Yasuda R, Nature 458, 299–304 (2009). [PubMed: 19295602]
30. Li B, Tadross MR, Tsien RW, Science 351, 863–867 (2016). [PubMed: 26912895]
31. Hollup SA, Molden S, Donnett JG, Moser M-B, Moser EI, J. Neurosci 21, 1635–1644 (2001). [PubMed: 11222654]
32. Dupret D, O'Neill J, Pleydell-Bouverie B, Csicsvari J, Nat. Neurosci 13, 995–1002 (2010). [PubMed: 20639874]
33. Pfeiffer BE, Foster DJ, Nature 497, 74–79 (2013). [PubMed: 23594744]
34. Sarel A, Finkelstein A, Las L, Ulanovsky N, Science 355, 176–180 (2017). [PubMed: 28082589]
35. Lavond DG, Kim JJ, Thompson RF, Annu. Rev. Psychol 44, 317–342 (1993). [PubMed: 8434892]
36. Eichenbaum H, Nat. Rev. Neurosci 15, 732–744 (2014). [PubMed: 25269553]

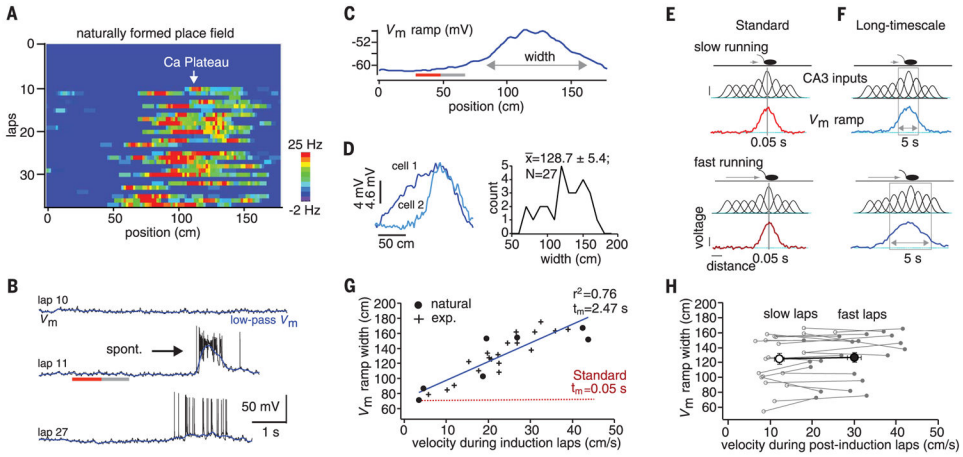

Fig. 1. Place-field properties suggest seconds-long plasticity rule.

(**A**) Spatial firing rates; (**B**) V_m (black) and low-pass filtered V_m (blue) for laps preceding (lap 10), during (lap 11), and after plateau (lap 14); and (**C**) average V_m ramp. Gray and red lines indicate the first 20 cm and preceding 20 cm of the V_m ramp, respectively. (**D**) Left, V_m ramps from two additional neurons (cells 1 and 2). Right, distribution of V_m ramp width for all recorded neurons. (**E**) Mouse on linear track for low (top)– and high (bottom)–velocity cases. Gaussian functions represent tuned input from CA3 neurons, where height indicates weight. Resulting V_m ramp for millisecond plasticity time window (gray box) is shown. (**F**) Same as in (E) except plasticity window covers seconds, allowing V_m ramp to vary as a function of running speed. (**G**) V_m ramp width versus average running velocity during induction trials. Data points fit by linear equation (blue line). Red dashed line is linear relationship expected for standard rule. exp., experimentally induced. (**H**) V_m ramp width versus average running velocity for laps after place-field induction. Slow laps (open symbols) and fast laps (closed symbols) for each neuron. Large open and closed circles are population means.

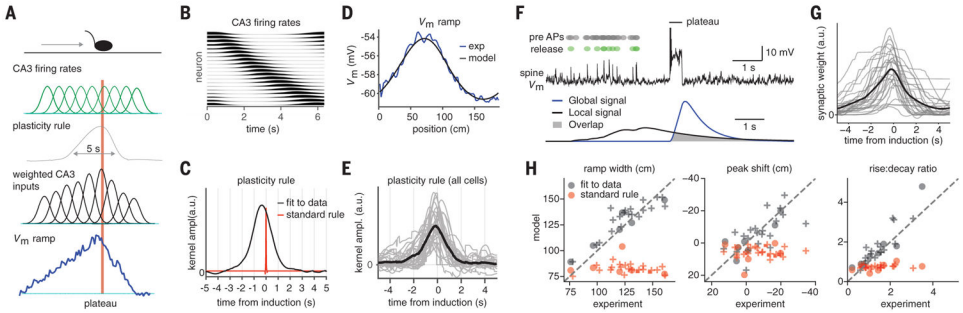

Fig. 2. Asymmetric synaptic plasticity rule spans for seconds around plateau potential.

(**A**) Mouse on linear track (top), Gaussian functions representing place-field firing in the CA3 neurons (green), the to-be-determined plasticity rule that controls the synaptic weights of CA3 inputs (gray), Gaussian functions representing CA3 excitatory input weighted by above rule (black), and the resulting V_m ramp in CA1 neuron (blue). Red bar indicates plateau potential. (**B**) Activity of CA3 population versus time during induction trial. (**C**) Synaptic weight values as a function of time from plateau (plasticity rule) inferred from the data (black) and 50-fold time-compressed rule (red) for comparison. ampl., amplitude; a.u., arbitrary units. (**D**) Measured V_m ramp (blue) compared with computed V_m ramp (black). (**E**) Inferred synaptic plasticity rule for all CA1 place cells. Black trace is mean. (**F**) Simulation of a CA1 pyramidal cell. Complex spike at track center induces plasticity. Top, CA3 place cell spiking (black dots), resulting glutamate release (green dots), and associated V_m in single CA1 spine (black trace). Bottom, calculated local spine signal (blue) and global dendritic signal (black). Overlap determines the synaptic-weight increment (gray). (**G**) CA3 synaptic input weight plotted relative to plateau initiation (gray, individual neurons; black, mean). (**H**) V_m ramps generated by signals reproduce the experimental data (gray), whereas the version that uses shorter signals does not (red). Naturally occurring (plusses) and experimentally induced plateaus (circles).

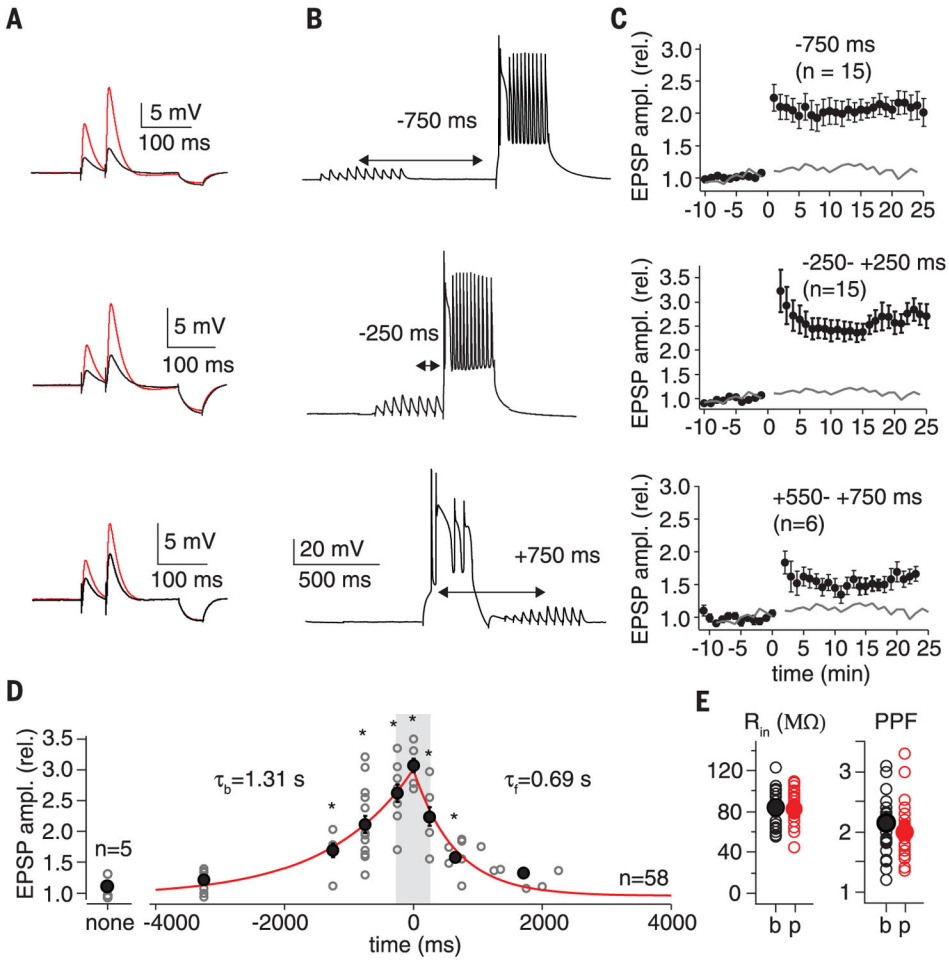

Fig. 3. Behavioral time scale synaptic plasticity.

(**A**) EPSPs used to determine synaptic strength (50-ms interval). Black trace is average baseline EPSP; red trace is average postpairing EPSP. Hyperpolarization following EPSPs from 50 ms, −25-pA current injection used to determine input resistance (R_{in}). (**B**) V_m trace showing representative induction protocol with 10 synaptic stimuli (20 Hz) followed by plateau potential (300-ms current injection). (**C**) Average EPSP amplitude (normalized to baseline; ±SEM) for population of neurons that received the indicated induction protocol. Induction (five pairings) at 0 min. Gray line is average EPSP amplitude for synaptic stimulation alone. (**D**) Plot of postinduction EPSP amplitude normalized to baseline versus the induction interval time for the entire population of neurons. Open gray symbols are individual neurons; black symbols are means. τ_b (tau backward) from exponential fit of data ranging from 0 to −3250 ms (red line projecting to negative times). τ_f (tau forward) from exponential fit of data ranging from 0 to +2000 ms (red line projecting to positive times). Synaptic stimulation alone (no pairing interval, labeled none) not included in exponential fits. See supplementary methods for means and *P* values. rel., relative. (**E**) R_{in} and paired-pulse facilitation (PPF) for baseline (b) and postinduction periods (p).

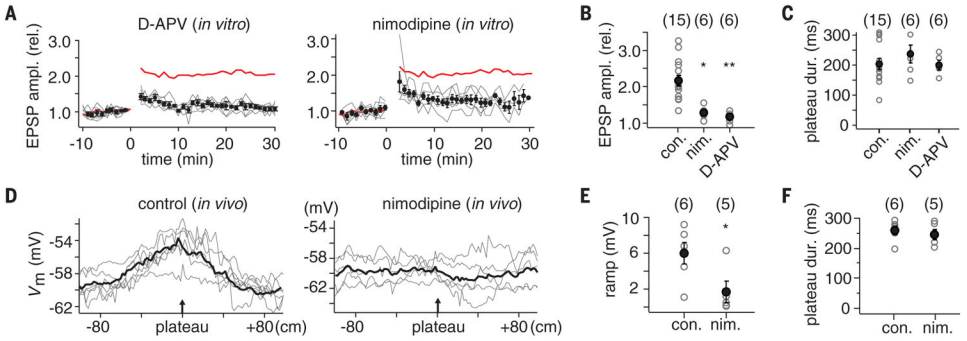

Fig. 4. Pharmacology of BTSP and place-field formation.

(**A**) Effect of 20 μM D-APV (left) and 10 μM nimodipine (right). Average EPSP amplitude (normalized to baseline; ±SEM) for population of neurons that received −750-ms interval induction protocol. Red line is mean for control [from (C)]. Gray lines are individual neurons. (**B**) Plot of EPSP amplitude (20 min postpairing/baseline) for control (con.), nimodipine (nim.), and D-APV conditions. **P* = 0.0011; ***P* = 0.00033. Number of cells in each group shown in parentheses. (**C**) Plot of average plateau-potential duration during the induction protocol for control, nimodipine, and D-APV conditions. No statistical differences were observed. (**D**) V_m ramp from individual neurons (gray traces) and the population average for control (left; pressure application of external solution containing vehicle) and for drug conditions (right; external solution containing 5 μM nimodipine). (**E**) Plot of V_m ramp amplitude induced for control and nimodipine conditions. **P* = 0.042. (**F**) Plot of average plateau-potential duration during the induction protocol for control and nimodipine conditions. No statistical differences were observed.